INTERACTION BETWEEN HIGH VOLTAGE SOLAR ARRAY AND ION THRUSTER PLASMA

Mengu Cho, Akiyo Saionji, Kazuhiro Toyoda
Kyushu Institute of Technology
Yukishige Nozaki
NEC Toshiba Space Systems, Ltd.
Tetsuo Sato
National Space Development Agency of Japan

Abstract

Recent solar arrays generate power at 100 V or higher. At the same time, ion thruster system is increasingly used on various spacecrafts. The ion thruster system emits dense plasma and the spacecraft is surrounded by Xe plasma whose density is often much denser than the ambient plasma. There is concern of plasma interaction between the dense Xe plasma that backflows to the solar array surface. Numerical simulations and laboratory experiments are carried out to investigate the interaction between solar array surface and Xe plasma that simulates the ion thruster backflow. Plasma density near the solar array produced by back flow charge exchange ions is calculated by a three-dimensional particle code. The threshold condition for anomalous electron current collection, so-called snap-over, are identified in the experiment.

Introduction

Since the end of last decade, satellites in geosynchronous (GEO) orbit have begun employing a bus voltage of 100 volts to match the demand for more power. At the same time the satellite size and the longer operational life time requires the mass-saving propulsion system such as electric propulsion, which is now widely used. In the past 5 years, the use of 100 volts solar arrays have widely spread among the GEO satellite because less plasma interaction is expected compared to LEO (Low Earth Orbit). The combination of high voltage solar array operating at a voltage of $100V$ or high and electric propulsion system, however, raises concern over the issue of plasma interaction.

The ion thruster neutralizer acts as a plasma contactor and the solar array has a positive potential with respect to the plasma and the spacecraft potential is nearly zero. The issue associated with solar array with a positive potential is electron current collection. The electron current is regarded as the leak of string current and corresponds to the loss of solar array power to the surrounding plasma. The collected current shows a sudden increase above a certain positive potential, which is called snapover [1, 2]. As the primary electrons strike the coverglass, one or more secondary electrons can be liberated. Many of these secondary electrons are collected by the exposed conductor, causing the current to increase dramatically [1, 2]. The gas-induced glow also occurs [2], once the ionization occurs inside the sheath near the conductive surface [3, 4]. The glow discharge results in a substantial power losses for spacecraft.

The increase of electron current to the solar array from the surrounding plasma may drop the solar array potential. If the collected electron current exceeds the amount of current emitted by the neutralizer (a fraction of an ampere, typically), it is possible that the spacecraft potential drops to a negative potential equal to the array output voltage $\simeq -100V$. If the neutralizer fails to operate, then the potential may drop to the beam acceleration voltage, $-1kV$, and this potential drop leads to arcing. Arcing at a high voltage solar array with a negative potential is due to the charging of the coverglass by ions from the surrounding plasma. Charging of the coverglass enhances the electric field at an interconnector, which is especially strong at the edges of the coverglass. The field enhancement

at the triple junction where the coverglass, interconnector and plasma meet leads to arcing [5]. Most of the case, an arc ends as a single pulse of discharge. But, when certain conditions are met, the arc plasma may short-circuit two points with different potentials on the strings of the solar arrays. When the solar array power is sufficient to sustain the arc, the solar array circuit may provide continuous energy to the arc plasma [6]. Such a state of arcing is called "sustained arc". Once a sustained arc occurs, it may destroy the array circuit causing the permanent loss of solar array power.

Cho *et al.* [7] carried out a laboratory experiments on solar array for the Engineering Test Satellite VIII (ETS8). The ETS8 is the first Japanese GEO satellite with 100V bus voltage and will be launched by NASDA in 2004. ETS8 will have two 12cm-diameter Kaufman type 20mN Xenon ion thruster. The plasma interaction between the Xenon plasma and solar array were investigated in a plasma chamber that produced similar plasma condition in orbit. In this paper, we present the results of the study carried out for solar array for Wideband InterNetworking engineering test and Demonstration Satellite (WINDS) that will be launched also by NASDA in 2005. Figure 1 shows a schematic image of the WINDS satellite. The satellite has two solar array paddles that generate more than $6.5kW$ after 5 years in orbit via approximately 11,000 triple junction cells. One wing of solar array paddle has a size of $7.5m \times 2.6m$. Originally the WINDS satellite planed to carry the same type of ion thrusters as ETS8. The principal axis of the thruster plume has an angle of 30 degrees from the axis of solar array paddle. The shortest distance from the ion thruster exit to the solar array paddle was about $4m$. Although later it was decided not to use the ion thrusters for the WINDS and the bus voltage of WINDS is 50V not 100V, the WINDS can be seen as an example of a typical GEO telecommunication satellite and the study method presented in this paper can be applied to other GEO satellites.

In the second and third sections of this paper we discuss computer simulations carried out to define the plasma conditions more precisely. The plasma density surrounding the solar array is the principal parameter that determines the degree of interaction, such as the amount of leak current or the arc rate. To carry out laboratory tests on the plasma interaction phenomena, realistic plasma parameters must be simulated on the ground. We have developed a three-dimensional computer simulation code to simulate the ambi-polar diffusion of the charge exchange ions and neutralizer electrons from the ion thruster plume. In the fourth section we present the results of laboratory tests to study the electron current collection. Finally we conclude the paper with discussion of future issues associated with a 300V bus voltage satellite employing an electric propulsion system.

Computer simulation

In Table 1 we list the parameters of ion thruster to be studied. The table lists for one thruster. During north-south station keeping, two thrusters are operated simultaneously. For the simulation, we make the following basic assumptions;

1. Pairs of electron and charge exchange ion are injected into the thruster plume so that the thruster plume has the steady density of charge exchange ion density, n_{cx}.
2. Beam ions are not considered.
3. We neglect collision between charged particles and neutral gas particles.
4. The satellite and the solar array have zero potential.
5. We neglect electric potential due to space charge of beam ions.
6. We consider the electric potential due to space charge of charge exchange ions and electrons.
7. The satellite size is one-hundredth of the real size.

The purpose of the simulation is to find out that the plasma density decreases by how many orders of magnitude near the solar array. Therefore, we put the priority on keeping the relative size of each component of the satellite. The simulation ignores several important parameters, such as presence of beam ions. The parameter affects the potential structure near the ion beam. If we include the

Parameter	Symbol	Value
Beam voltage	V_b	1000V
Specific Impulse	I_{sp}	2500s
Thrust	F	22mN
Beam current	I_b	0.42A
Propellant mass flow rate	Γ	9.1sccm
Thrust efficiency	η_T	0.93
Propellant utilization efficiency	η_f	0.69
Thruster exit radius	r_b	0.06m
Thruster exit area	A_e	0.0113m^2
Mass flow rate	$\dot{m}$	8.3×10^{-7} kg/s
Neutral thermal speed	v_n	140m/s

Table 1: Ion thruster parameters

beam ions, the results could be different from the one presented here. Nevertheless, the purpose of the present simulation is to find adequate experimental conditions. An estimate on the order of magnitude suffices that purpose.

In the present simulation, we use a full particle scheme where electrons and ions are both treated as particles. In the past, the simulations of ion thruster plume [8] were done mostly using a hybrid scheme where only ions were treated as particles and electrons were treated as fluid. In the hybrid scheme electron density is calculated by the bolztman distribution, $n_e = n_o \exp(-e\phi/\kappa T_e)$, where ϕ is the negative potential and n_o is the plasma density of the highest potential, that is $\phi = 0$. Therefore, in the hybrid scheme we first need to determine the point of highest potential, which is usually the thruster exit. One disadvantage of the hybrid scheme is that we have to integrate the nonlinear Poisson equations. In the full particle scheme, we can use the Fourier transform if the numerical grids are evenly spaced. With the use of capacitance matrix methods [9] to calculate the body potential, the Poisson equation can be solved without any iteration. The use of a full particle scheme also leaves a room of expansion for the future study where the sheath from the solar array paddle is no longer neglected, such as a 300V bus satellite. The hybrid scheme cannot be applied if there is any point in the computational domain with a potential more positive than the reference point.

We first need to estimate the charge exchange ion density inside the thruster plume. In the coordinate system shown in Fig. 2, the neutral density distribution is modelled by

$$n_n(x,r) = n_{no}\frac{(x+r_t)}{((x+r_t)^2+r^2)^{3/2}}r_t^2 \tag{1}$$

where n_{no} is the neutral density at the thruster exit that is given by

$$n_{n0} = \frac{\dot{m}(1-\eta_f)}{Mv_nA_e} = 7.4\times10^{17}m^{-3}. \tag{2}$$

Equation 1 follows the modelling done by Samtaroy *et al.* [8]. Also following the modelling of Ref. [8], we model the beam ion density distribution by

$$n_{bi}(x,r) = \frac{2I_b}{ev_b\pi r_b^2}\left(1-\frac{r^2}{r_b^2}\right) \tag{3}$$

where r_b is the beam radius at a distance x given by

$$r_b = r_t + xtan\theta. \tag{4}$$

The ion density inside the thruster plume was measured previously in Ref. [11]. The ion densities at the plume axis were $2\times10^{15}m^{-3}$ at $x = 0.5m$ and $8\sim9\times10^{14}m^{-3}$ at $x = 1m$. In order to match theses densities and the width of ion beam measured in Ref. [11], we choose $\theta = 12.5^o$ as the thruster cone angle.

Once we know the neutral density and the ion density inside the thruster plume, we can calculate the rate of production of charge exchange ions, that is given by

$$\dot{N}_{cx} = \int_0^x \int_0^{r_b} n_{bi} n_n \sigma_{cx} v_b 2\pi r dr dx = \frac{4 n_{no} I_b \sigma_{cx} r_t^2}{e} f(x) \tag{5}$$

where $f(x)$ is a function of x denoted by

$$\int_0^x \int_0^{r_b} \frac{(x' + r_t)}{(x' + r_t)^2 + r^2)^{3/2}} \frac{1}{r_b^2} \left(1 - \frac{r^2}{r_b^2}\right) r dr dx'. \tag{6}$$

The function $f(x)$ becomes almost flat beyond $4m$ as shown in Fig. 3, meaning that most of CEX ions are produced at $x < 4m$.

We consider volumes subdividing the thruster plume as shown in Fig. 4. Each volume has an outer surface area of $S(x)$ depending on the distance from the thruster exit, x. At the steady state, the number of CEX ions escaping the volume with the surface area, S, per unit time is equal to the number of CEX ions generated within the volume per unit time. Therefore, we can write

$$n_{cx}(x) \sqrt{\frac{\kappa T_e}{m_i}} S(x) = \frac{4 n_{no} I_b \sigma_{cx} r_t^2}{e} \left(f(x + \delta x) - f(x)\right) \tag{7}$$

where the volume occupies between x and $x + \delta x$ on the thruster axis. The left hand side of Eq. 7 is calculated from the assumption of ambipolar diffusion. We consider 6 boxes of diffusion source along the thruster axis. Because the simulation coordinate is rectangular, we model the volume by rectangular boxes. From Eq. 7, we can calculate the density of CEX ion at each diffusion source and plot the result in Fig. 5. In the calculation, we assume $3eV$ as the electron temperature from Ref. [11]. We assume inside each rectangular box, the densities of charge exchange ions are kept at the values shown in Fig. 5, where we use Ref. [10] for the charge exchange collision cross-section, σ_{cx}. Using the right hand side of Eq. 7, we calculate the number of CEX ions produced within one time step. At each time step, we inject that number of ion and electron pair into each diffusion source.

As shown in Fig. 5, the density at the thruster exit is larger than $10^{13} m^{-3}$. The debye length at this plasma condition is approximately $3mm$. As it is well known, the grid size of PIC code is limited to one Debye length [12]. Therefore, in order to model the whole body of the satellite with $\Delta x = 3mm$, we need a huge number of computational grids. In order to avoid this problem, we reduce the size of satellite to one-hundredth the real size while assuming the plasma of densities given in Fig. 5 and the temperature of $3eV$ at the diffusion sources. This means that the satellite modelled in the simulation is a miniature model of 100th scale compared to the real satellite.

In Fig. 6 we show the 100th scale model used in the simulation. It should be noted that x axis is now perpendicular to the body with 60 degrees from the principal axis of the thruster plume. The satellite structure is simplified so that only the major elements of the satellite shape remains, such as body, antennas, and solar array paddles, which are shown in dark green. The diffusion sources are also shown in light green. In the figure the size is given in meter. The computational domain consists of $64 \times 128 \times 48$ grids. The outer boundary is fixed to zero potential. Once a particle reaches the outer boundary or the satellite surface, it is removed from the domain. The ion-to-electron mass ratio is 100. This mass ratio is much smaller than the real mass ratio of Xe ions. As long as the purpose of the simulation is to find out the steady state density distribution, the use of artificial mass ratio is justified. The simulation is started with particles in the diffusion source only and stopped when the number of particles inside the domain reaches the steady value.

Simulation result

Figure 7 shows the computational result when the solar array paddle is facing x axis. In the figure, the isosurface where the density is $5 \times 10^{10} m^{-3}$ is shown in yellow color. The scatter of green points are the artifact due to the computer visualization software. The two ion thrusters are located at $+x$ and $-x$ surface of the body. In this case, each side of the solar array paddle sees only one thruster.

The CEX ions diffusing from the thruster plume in $+x$ or $-x$ direction reaches the paddle surface. Figure 8 shows the distribution of the ion density on xy plane at $z = 0.072mm$ that crosses the center of the solar array paddle. Strictly speaking, the satellite structure is not symmetric across y axis because of the antennas located at the upper portion of the body. The presence of antennas, however, affects little on the distribution of ion density. The density distribution is symmetric across y axis and almost radial from the satellite body except near the thruster exit.

In Fig. 9 we plot the ion density along the y axis crossing the thruster exit on the xy plane shown in Fig. 8. The ion density over the solar array paddles is of the order of $10^{10}m^{-3}$. The maximum is $7.6 \times 10^{10}m^{-3}$ at the edge facing the thruster exit. Figure 10 shows the similar distribution as Fig. 8 but for the case where the solar array paddle faces z axis. In Fig. 10 the distribution of ion density is shown on xy plane at $z = 0.075mm$, one grid over the solar array paddle. In this case the ions diffusing from the two plumes can mix over the solar array paddle. Then the density over the paddle is more uniform than the case shown in Fig. 8. In Fig. 11, where the ion density is plotted along y axis crossing the thruster exit on the xy plane shown in Fig. 10. The maximum value, $7.2 \times 10^{10}m^{-3}$, is a little smaller than the other case, but the distribution is more uniform over the solar array.

In conclusion, when the ion thrusters are operated for north-south station keeping, the maximum plasma density near the solar array is $7.6 \times 10^{10}m^{-3}$ at maximum. It is a coincidence that the values are similar to the plasma density in Low Earth Orbit. From these simulations, the laboratory tests are carried out under the plasma density of the order of $10^{11}m^{-3}$, giving a safety margin.

Laboratory test

Because most part of the solar array has a positive potential with respect to the plasma, we focus our tests on measurement of plasma leakage current from a solar array coupon biased positively. A solar array panel coupon has been fabricated with the same procedure as the flight product. We show a photograph of coupon in Fig. 12. The coupon has three strings of triple-junction cells of $7.6cm \times 3.7cm$. In one string, five cells are connected in series. The solar array strings are mounted on top of Kapton sheet over aluminum/CFRP substrate. At the back side of the coupon, a blocking diode board is mounted to simulate the flight condition. All the four edges around a cell is coated by RTV silicon to prevent arc discharge during substorm condition based on the previous study [7]. The bus bar is also coated by RTV. Therefore, the strings expose the conductive part only at the interconnectors.

The detail of experimental set-up is given in Ref. [7]. Xenon plasma is produced by an electron-cyclotron-resonance plasma source. The plasma density at the solar array during the experiment is $1 \times 10^{11}m^{-3}$ and the electron temperature is $1 \sim 2eV$. The typical chamber pressure is $4 \times 10^{-4}Torr$. The three strings are combined and biased to a positive potential by a DC power supply. The diode board is also biased, while the aluminum/CFRP substrate is grounded. The electron current flowing to the string circuit from the surrounding plasma is measured.

Figure 13 shows the current collected for different bias voltage. We see a jump in the current collection at $170V$, which indicates the snapover. In the same figure we also plot the results of the tests carried out for ETS-VIII solar array coupons [7]. In Ref. [7] we tested two types of solar array coupon similar to the one used for the present study, though the strings are made of $7cm \times 3.5cm$ Si cells. The coupon W/RTV had its bus bars coated by RTV-Si like the present coupon. Most of the cell edges was also coated by RTV. The coupon W/O/RTV didn't have coating on the bus-bar nor at the cell edges. The result of the WINDS coupon lies between W/RTV and W/O/RTV coupons of ETS-VIII. The majority of the exposed metallic area for the W/O/RTV coupon was bus-bar. Although the bus-bar of the WINDS coupon was coated by RTV, the diodes at the back side had lead wires exposed to the plasma. Therefore, the WINDS coupon collected electrons not only at interconnectors but also at the diodes. The area of the exposed metallic surface of the diode board was not as large as the exposed area of bus-bar. That's why the WINDS coupon collected more electrons than the W/RTV coupon but less than the W/O/RTV coupon.

The electron current collection at the diodes was verified by observation of glow discharge at the diodes. As the bias voltage was increased to near 200V, the current suddenly increased further to tens of milliampere. The glow discharge occurs as repeated pulses with the repetition rate of several pulses

per 1 ms. The glow discharge is due to ionisation inside the sheath surrounding the positively biased metallic surface. In Fig. 14, we show the inception voltage of glow discharge for different neutral density. In the figure we also show the result of ETS-VIII solar array coupon [7]. For larger area of exposed metallic surface, the glow discharge occurs at lower voltage. Generally the higher the neutral density, the lower the glow discharge inception voltage, though the WINDS coupon has more or less the same inception voltage of $170 \sim 200V$ for the neutral densities investigated.

From the laboratory test results, we can deduce the amount of leakage current expected in orbit. The WINDS coupon collected $0.01mA$ for 15 cells. The WINDS satellite has a total of 11000 cells. Therefore, the amount of power lost due to the leakage current is only $0.4W$, which is a tiny portion compared to the total power generated by the solar array, $6.5kW$. It should be noted that for the real satellite, the number of diode boards is limited. Therefore, the diode board occupies little fraction of the electron current collected by the entire solar array paddle. Therefore, even the estimate of $0.4W$, which is based on the result of 15 cells and one diode-board, is an overestimate. Therefore, under the normal condition there is no need to worry about the current leakage.

There is a chance, however, that an accidental increase of neutral gas density near the solar array induces the glow discharge. The neutral density can be increased due to thruster firings. For the case of WINDS, the possibility of glow discharge inception in orbit is negligible from the facts that the glow inception voltage was $170V$ in laboratory and the maximum neutral density near the solar array expected in orbit is of the order of $10^{16}m^{-3}$.

Only arcing at the event of neutralizer failure would be left as an issue. Once the neutralizer fails, the satellite potential rapidly drops to a negative potential comparable to the beam voltage $\sim -1kV$. Then the ions charge the coverglass surface. There is always a safety circuit in the ion thruster power system that automatically switch-offs once the failure of neutralizer is detected. For the case of the WINDS satellite, it takes several milliseconds to switch-off the power. If not only CEX ions but also beam ions contribute to the charging of coverglass, the potential difference between the interconnector and coverglass can reach to as high as 600V even during this short time scale, which is enough to cause an arc. Then the arc plasma might short-circuit the solar array string circuit. For the case of WINDS, the gap between solar array strings are grouted by RTV-Si to prevent short-circuit between the adjacent strings. The Kapton sheet under the interconnector is also covered by RTV to prevent short-circuit between string and substrate. These are the precautions already taken against arcs expected to occur during substorm condition, which is more likely than the neutralizer failure. Therefore, even if an arc occurs due to the failure of neutralizer, it will ends as a pulse of arc that causes little harm .

conclusion

Plasma environment near a geosynchronous satellite with ion thruster system has been calculated via computer simulation. As a typical example of GEO satellite, the WINDS satellite has been chosen. During the ion thruster operation for north-south station keeping, the ion density near solar array paddles reaches near $10^{11}m^{-3}$, which coincide with the plasma density at LEO.

Charge exchange ions diffuse backward via ambipolar diffusion from the thruster plume to the satellite body and the solar array paddle. Because the neutralizer acts as a plasma contactor, the satellite potential is kept the same as the neutralizer electrons. Therefore, most of the solar array has a positive potential with respect to the plasma. In that case the main issue of plasma interaction is the current leakage and power loss due to electron current collection at the exposed metallic surface of the solar array. The larger the exposed metallic surface, the more current the array collects. The power loss is negligible, however, as long as the surrounding gas density is kept low so that no gas-induced glow discharge occurs. The inception voltage of glow discharge is well above 100V, giving enough safety margin to a satellite with 100V solar array. Thus the only precaution to be taken against the plasma interaction is the suppression of sustained arc which might occur at the event of neutralizer failure. Because only one or two arcs are expected to occur while the satellite potential drops to a highly negative value, precautions taken against substorm suffices for such a rare case.

For a satellite with 300V or higher bus voltage, however, the conclusion is different. Currently, development of 300V bus is underway, to realize the direct drive of electric propulsion system, mainly

a hall thruster. At 300V, the power loss for a typical 10kW class GEO satellite can be of the order of 100W, even if most of the metallic surface is covered by the insulative layer. The glow discharge occurs at a voltage of as low as 300V at the neutral density of $\sim 10^{18} m^{-3}$. Once a glow discharge occurs and the current exceeds the maximum current provided by the neutralizer, the satellite and solar array potential may drop to $-300V$ with respect to the surrounding plasma. Then arcing becomes a serious issue, because it would be no longer one-time only phenomena such as the neutralizer failure.

Modelling of plasma environment around a 300V bus satellite with an electric propulsion system is also challenging. In the present paper the solar array surface has been assumed to be zero potential. This assumption is valid as long as the sheath from the metallic surface is sufficiently thin so that the sheath boundary does not overlap the thruster plume. But as the voltage increases and the sheath boundary extends further, it may overlap the thruster plume. Then the motion of CEX ions is no longer modelled as ambipolar diffusion. The sheath from the solar array distorts the potential structure of the thruster plume edge and affects the motion of neutralizer electrons as well as CEX ions. We can no longer use the hybrid scheme that requires all the computational domain to be negative with respect to the point with the quasi-neutral density, n_{n0}. A full particle scheme that incorporates the potential structure of thruster plume and the sheath from the solar array will become necessary.

References

[1] Hastings, D. E., and Chang. P., "The Physics of Positively Biased Conductors Surrounded by Dielectrics in Contact with Plasma", *Physics of Fluids B*, Vol.1, 1989., pp.1123-32.

[2] Galfaro,J.T.,Ferguson,,D.C.,Vayner,B.V.,Degroot,W.A.,Thomson,C.D.,Deninson,J.R., and Davies, R. E., "Inception of Snapover and gas Induced Glow Discharges", *AIAA paper 2000-0245*, January, 2000.

[3] Cooke, D. L. and Katz, I., "Ionization-Induced Instability in an Electron Collecting Sheath," *J. Spacecraft and Rockets*, Vol.25, No.2, 1988, pp.132-138.

[4] Cho, M., "Ionization around a High Voltage Body in Magnetized Non-flowing Ionospheric Plasma," *J. Spacecraft and Rockets*, Vol.35, No.1, 1998, pp.90-99.

[5] Hastings, D.E., Cho, M., and Kuninaka, H., "The Arcing Rate for a High Voltage Solar Array: Theory, Experiment and Predictions," *J.Spacecraft and Rockets*, Vol. 29, No.4, 1992., pp.538-554.

[6] Katz, I., Davis, V.A; and Snyder, D.B; "Mechanism for Spacecraft Charging Initiated Destruction of Solar Arrays in GEO," *AIAA paper 98-1002*, January 1998.

[7] Cho, M., Ramasamy, R., Toyoda, K., Nozaki, Y., and Takahashi, M., "Laboratory Tests on 110-Volt Solar Arrays in Ion Thruster Plasma Environment" *J. Spacecraft and Rockets, to be published*, 2003.

[8] Samanta Roy, R., and Hastings D.E, "Three-Dimensional Modeling of Dual Ion-Thruster Plumes for Spacecraft Contamination", *J.Spacecraft and Rockets*, Vol. 33, No.4, 1996., pp.519-524.

[9] Hockney, R.W., and Eastwood, J.W, "Computer Simulation using Particles", *IOP Publishing Ltd.*, New York, 1988.

[10] Rapp, D., and Francis, W.E., "Charge Exchange Between Gaseous Ions and Atoms", *J. Chemical Physics*, Vol.37, No.11, 1962, pp.2631-2645.

[11] Ozaki, T., Kajiwara, K., Tsujihata, A., and Takahashi, M., "Plasma Diagnosis in the Plume of the 20mN Ion Thruster for ETS-8", *Proceedings of 7 th Spacecraft Charging Technology Conference* April 2001.

[12] Birdsall, C. K., and Langdon, A. B., "Plasma physics via computer simulation", *Mcgraw-Hill*, New York, 1985.

Figure 1: Schematic picture of the WINDS satellite.

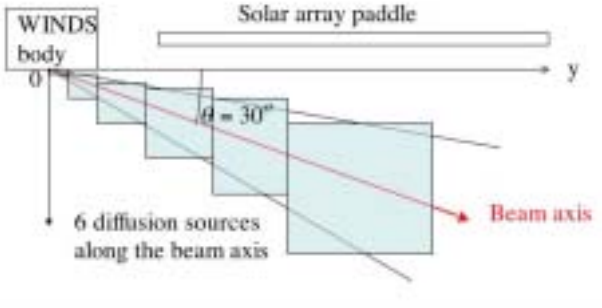

Figure 4: Schematic picture of diffusion source along the thruster plume.

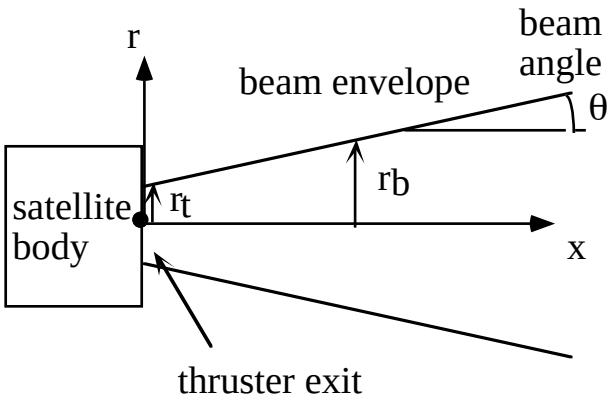

Figure 2: Coordinate system used to calculate the distribution of beam ion and neutral density inside the thruster plume.

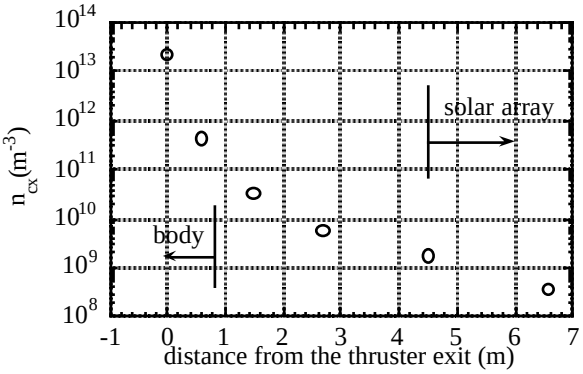

Figure 5: Density of CEX ions at each diffusion source along the thruster plume. The distance is along y axis shown in Fig. 4

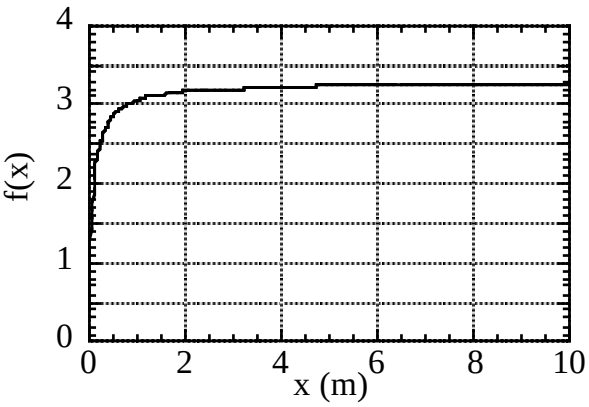

Figure 3: Plot of $f(x)$ defined in Eq. 6.

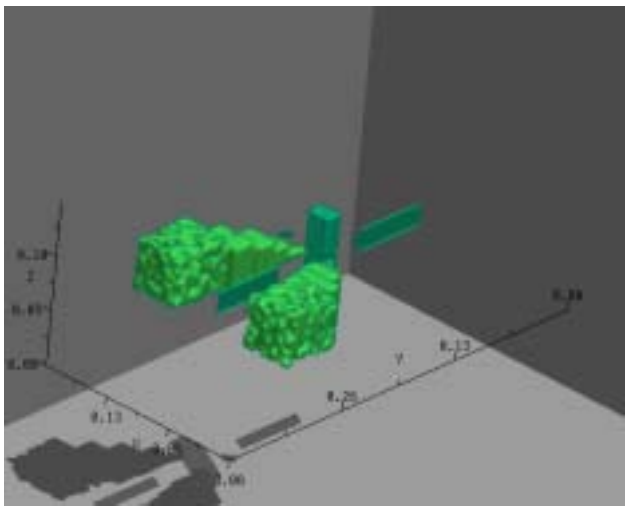

Figure 6: Computational model of the WINDS satellite.

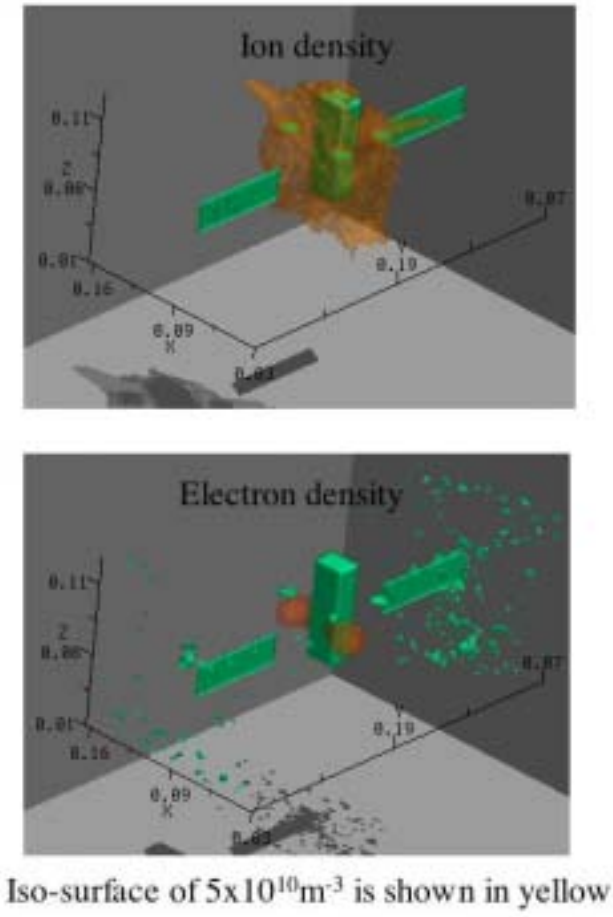

Figure 7: Ion and electron densities around the WINDS satellite.

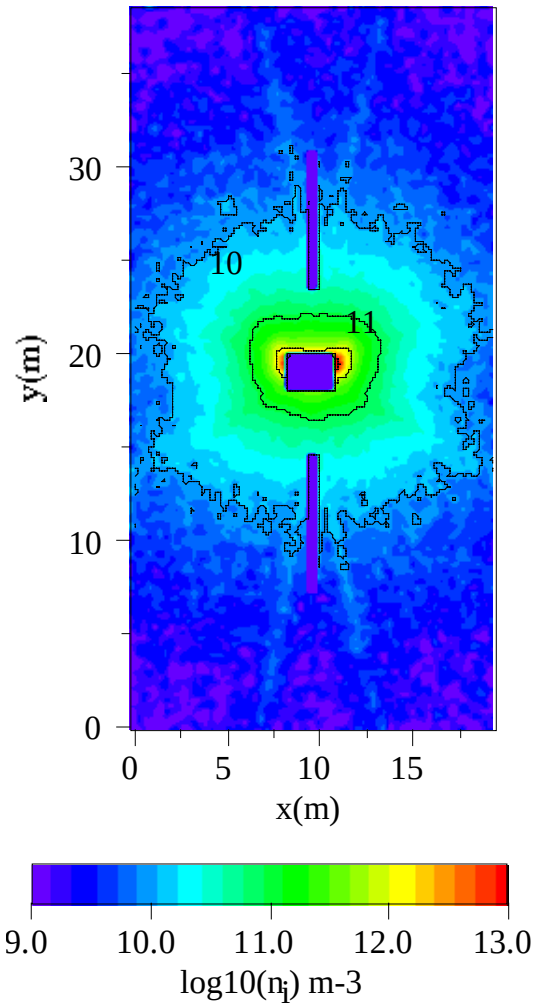

Figure 8: Distribution of ion density on xy plane when the solar array paddle faces the x axis.

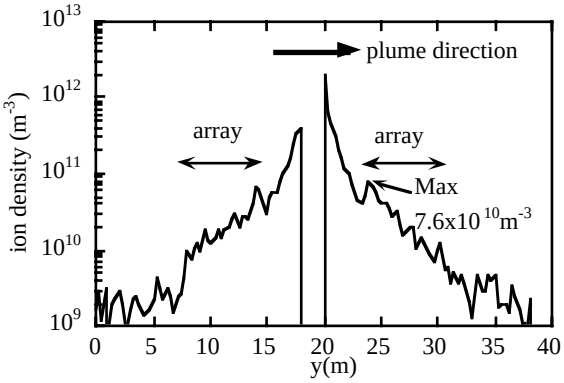

Figure 9: Distribution of ion density along y axis crossing the thruster exit on xy plane shown in Fig. 8w

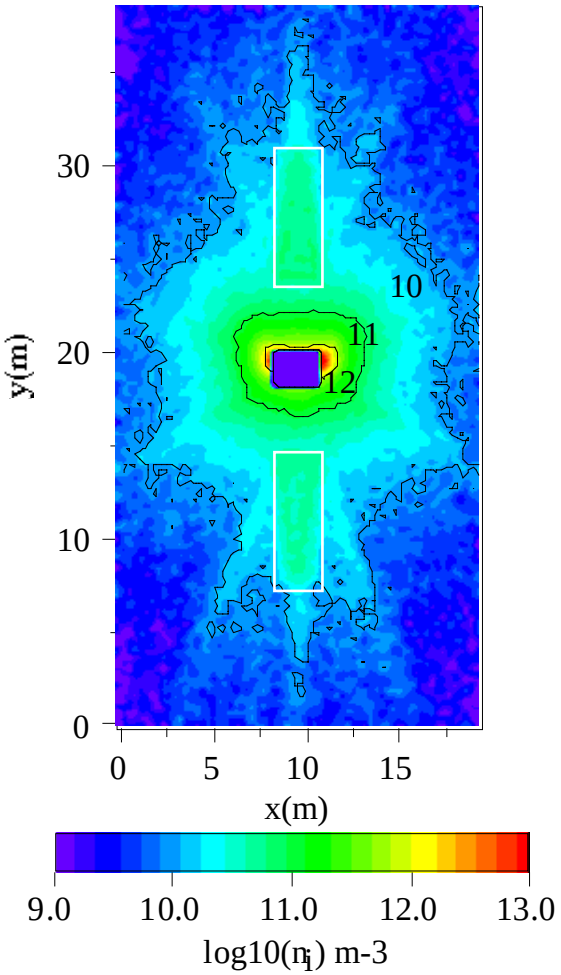

Figure 10: Distribution of ion density on xy plane when the solar array paddle faces the z axis.

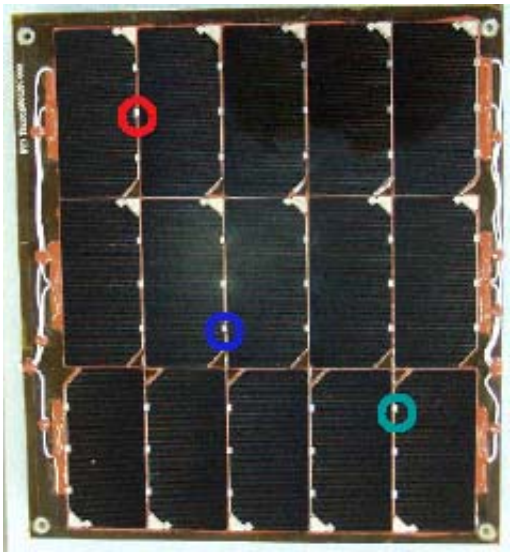

Figure 12: Photograph of solar array coupon used in the laboratory experiment.

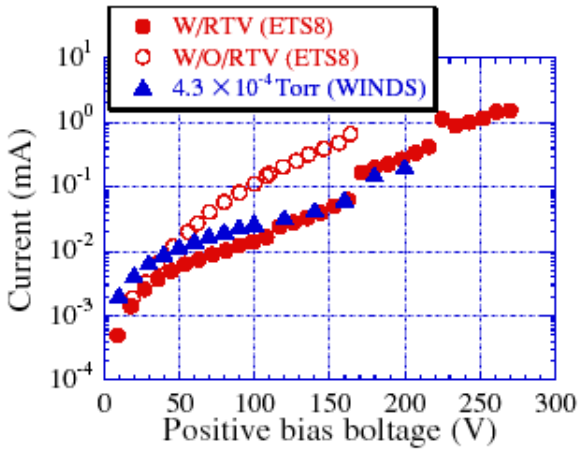

Figure 13: Electron current collected at different bias voltages.

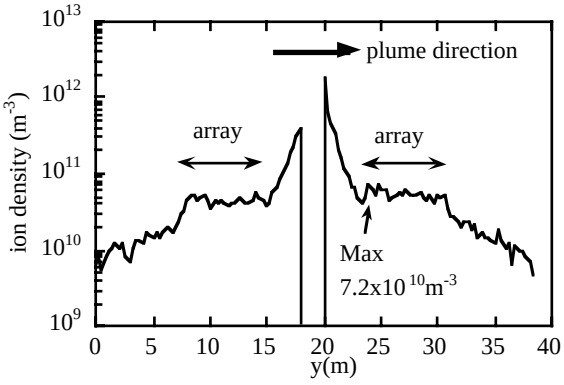

Figure 11: Distribution of ion density along y axis crossing the thruster exit on xy plane shown in Fig. 10

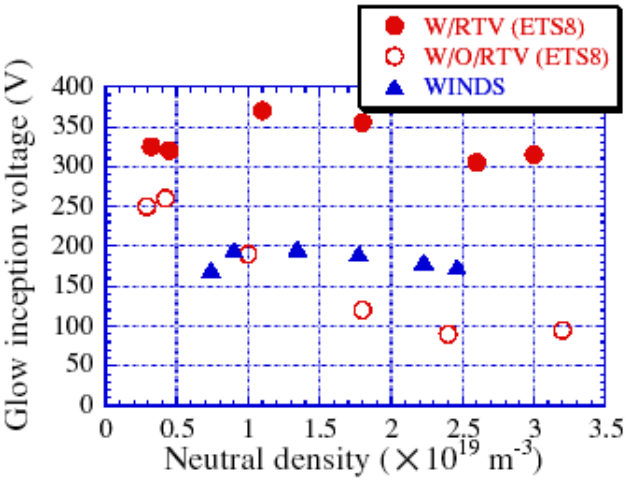

Figure 14: Glow inception voltage for different neutral density